Heat treatment effects on Fe_3O_4 nanoparticles structure and magnetic properties prepared by carbothermal reduction

Ping Hu [a], Shengen Zhang [a,*], Hua Wang [b], De'an Pan [a], Jianjun Tian [a], Zhi Tang [a], Alex A. Volinsky [c]

[a] School of Materials Science and Engineering, University of Science and Technology Beijing, Beijing 100083, China
[b] Tianjin Heavy Equipment Engineering Research Co. Ltd., China First Heavy Industries, Tianjin 300457, China
[c] Department of Mechanical Engineering, University of South Florida, Tampa, FL 33620, USA

ABSTRACT

Fe_3O_4 nanoparticles were prepared by carbothermal reduction method using glucose as carbon source. Heating temperature and holding time effects on crystalline phase composition and magnetic properties of Fe_3O_4 nanoparticles were investigated by X-ray diffraction, field-emission scanning electron microscopy and vibrating sample magnetometer. Pure Fe_3O_4 nanoparticles with an average crystallite size of 48 nm was obtained at higher heating temperature of 650 °C and shorter holding time of 0.5 h, or at lower heating temperature of 450 °C and longer holding time of more than 6 h. The crystallite size of Fe_3O_4 nanoparticles increases with heating temperature and holding time. Fe_3O_4 nanoparticles heated at 650 °C for 2 h have the highest saturation magnetization (M_s = 97.99 emu g^{-1}), higher than Fe_3O_4 prepared by other techniques due to better microstructure, crystallinity and expanded crystalline cell.

© 2010 Elsevier B.V. All rights reserved.

1. Introduction

Magnetite (Fe_3O_4) is an important magnetic material that is widely used in different applications such as magnetic sensors [1], high density magnetic recording media [2], printing ink [3], ferrofluids [4], magnetic resonance imaging [5], catalysts [6] and especially in the biomedical field [7,8] due to its chemical stability and biocompatibility. There have been several methods reported to synthesize Fe_3O_4 powders, including co-precipitation [9], oxidation of $Fe(OH)_2$ by H_2O_2 [10], microemulsion [11], hydrothermal synthesis [12], sol–gel method [13], thermal decomposition of alkaline solution of Fe^{3+} chelate in the presence of hydrazine [14], pyrolysis of EDTA ferric sodium salt [15], reduction of hematite by CO [16], and organic solution phase decomposition of $Fe(cup)_3$, $Fe(acac)_3$, or $Fe(CO)_5$ [17–19]. However, some of these methods encountered problems with complicated equipment and/or long preparation time caused by multiple processing steps, deeming them economically unfeasible for large-scale production.

In previous work Fe_3O_4 powders were successfully synthesized from Fe_2O_3 powder and glucose mixture as starting materials using a novel carbothermal reduction method [20]. The effects of glucose mole fraction on crystalline phase composition and carbothermal reduction mechanisms were studied. In this paper temperature and holding time effects on the structure and magnetic properties

of Fe_3O_4 nanoparticles by carbothermal reduction method were investigated.

2. Experimental procedure

Fe_2O_3 powder was prepared as a carbothermal reduction raw material by citrate–nitrate precursor auto-combustion method, which allowed producing ultrafine powders with chemically homogeneous composition, uniform size and good reactivity [21]. Ferric nitrate ($Fe(NO_3)_3 \cdot 9H_2O$) and citric acid ($C_6H_8O_7 \cdot H_2O$) were dissolved in de-ionized water, and the solution pH value was adjusted to 7.0 using $NH_3 \cdot H_2O$. The solution was heated to 60 °C and continuously stirred using magnetic agitation. After 4 h, the solution became a homogeneous brown sol. Then the sol was dried at 120 °C in an oven for 12 h and became a brown dry gel. Dry gel was ignited in air and spontaneously combusted, producing loose, red-brown and very fine Fe_2O_3 powder.

Glucose (1/24 fixed mole fraction) was mixed with Fe_2O_3 powder used in experiments [20]. The mixture was heated between 400 °C and 700 °C for different holding times in the tube furnace with argon atmosphere for carbothermal reduction reaction.

X-ray powder diffraction (XRD) patterns were recorded using Philips APD-10 X-ray diffractometer with Cu Kα radiation. The morphology and size of particles were observed in field-emission scanning electron microscope (FE-SEM, ZEISS ULTRA 55, Germany). Magnetic properties measurements were carried out in a vibrating sample magnetometer (LDJ 9600, LDJ Electronics, USA).

3. Results and discussion

3.1. Temperature effect on phase composition

In order to investigate the influence of heating temperature on samples' phase composition, mixture of glucose and Fe_2O_3 powder was heated at different temperatures ranging from 400 °C to 700 °C

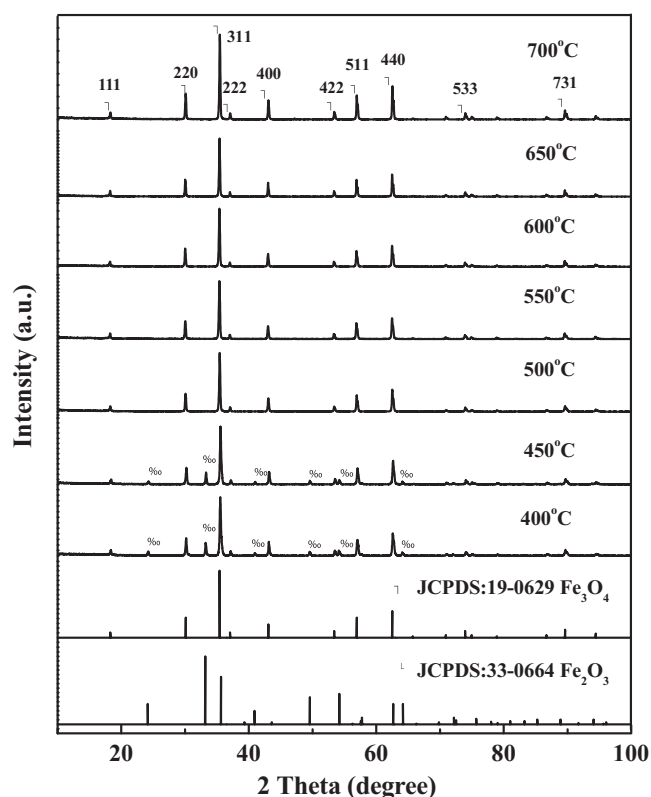**Fig. 1.** XRD patterns of samples heated for 2 h at different temperatures.

Fig. 2. XRD patterns of samples heated at 450 °C with different holding times.

for 2 h. XRD patterns of heated samples are shown in Fig. 1. Above 500 °C products have pure Fe_3O_4 phase (JCPDS: 19-0629) with all detectable diffraction reflections well indexed as pure cubic spinel phase and no impurities diffraction is observed in the patterns. However, powders have Fe_2O_3 impurity phase (JCPDS: 33-0664) when heated below 500 °C for 2 h.

Previous results show that glucose is the source of carbon and CO gas, which both react with Fe_2O_3 to form Fe_3O_4 [20]. Carbon content and CO concentration determine the carbothermal reduction reaction ratio. Pyrolysis temperature of glucose is about 364 °C determined by thermogravimetric and differential thermal analysis (TG-DTA) [20]. Glucose was continuing to decompose between 400 °C and 500 °C. Therefore, below 500 °C, only mixed Fe_3O_4 and Fe_2O_3 powders were obtained due to a lack of carbon. Low carbon sources cannot reduce Fe_2O_3 to Fe_3O_4 completely. The average crystallite sizes were determined using the Scherrer formula. The crystallite size of samples increases with the heating temperature and holding time.

3.2. Holding time effect on phase composition

Since pure Fe_3O_4 could not be obtained after 450 °C exposures for 2 h, heating was prolonged up to 8 h. XRD patterns of heated samples with different holding times at 450 °C are shown in Fig. 2. Heated samples did not reduce completely and have Fe_2O_3 impurity phase when the holding time is less than 6 h at 450 °C. However, pure Fe_3O_4 phase can be obtained when the holding time is longer than 6 h due to simulative decomposing of glucose for prolonged holding time.

From another perspective, glucose and Fe_2O_3 powder mixture were heated to 650 °C for shorter holding time of 0.5 h. XRD patterns of heated samples with different holding times at 650 °C are shown in Fig. 3. At 650 °C, even for 0.5 h, pure Fe_3O_4 phase was obtained due to an adequate decomposed carbon source at this temperature.
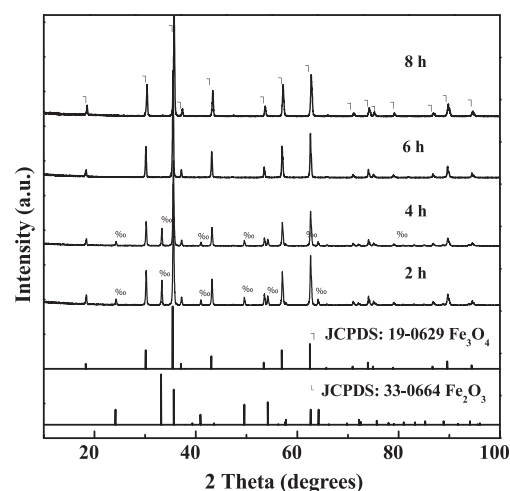
Therefore, pure Fe_3O_4 phase can be obtained at higher heating temperature (650 °C) and shorter holding time (even 0.5 h), or at lower heating temperature (450 °C) and longer holding time (longer than 6 h).

3.3. Morphology characterization

Typical FE-SEM micrographs of Fe_3O_4 nanoparticles' microstructure at 650 °C and 700 °C for 2 h are shown in Figs. 4 and 5, respectively. Fig. 4 shows that spherical Fe_3O_4 nanoparticles obtained by this method are uniform in both morphology and size, but agglomerate to some extent. The average diameter of prepared Fe_3O_4 nanoparticles is about 45 ± 2 nm with narrow size distribution, which is close to the crystallite size estimated from the Scherrer formula of the XRD pattern. However, more aggregation and even partial sintering occur at a higher temperature of 700 °C for 2 h is shown in Fig. 5.

3.4. Magnetic properties

Magnetic properties of Fe_3O_4 nanoparticles were studied using a vibrating sample magnetometer (20 kOe magnetic field) at room temperature. Magnetic hysteresis curves for Fe_3O_4 nanoparticles processed at different conditions are shown in Fig. 6. The upper left
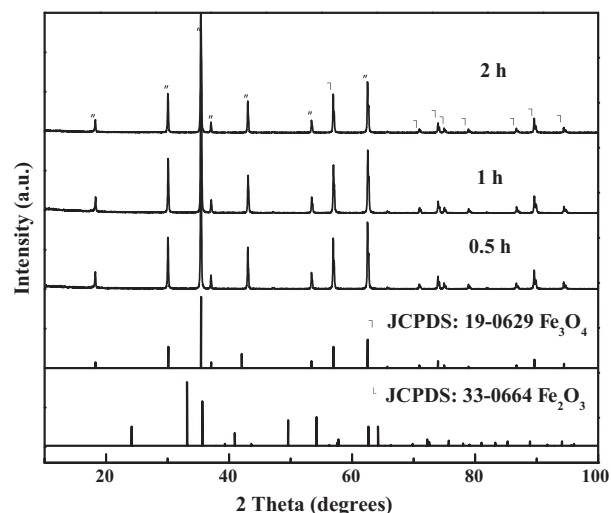

Fig. 3. XRD patterns of samples heated at 650 °C with different holding times.
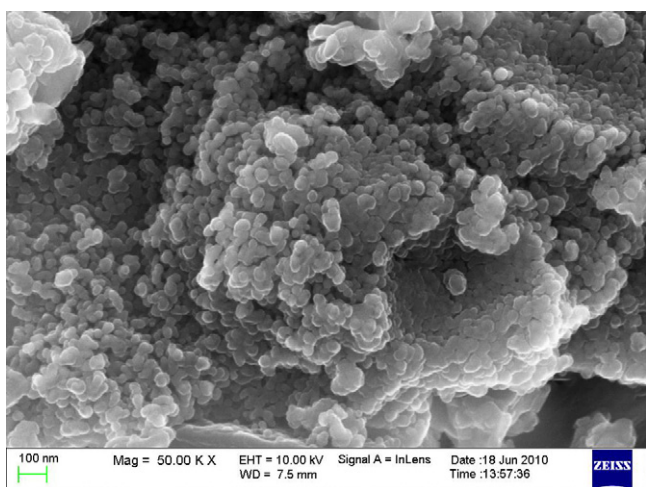
Fig. 4. FE-SEM micrograph of Fe_3O_4 nanoparticles heated at 650 °C for 2 h.

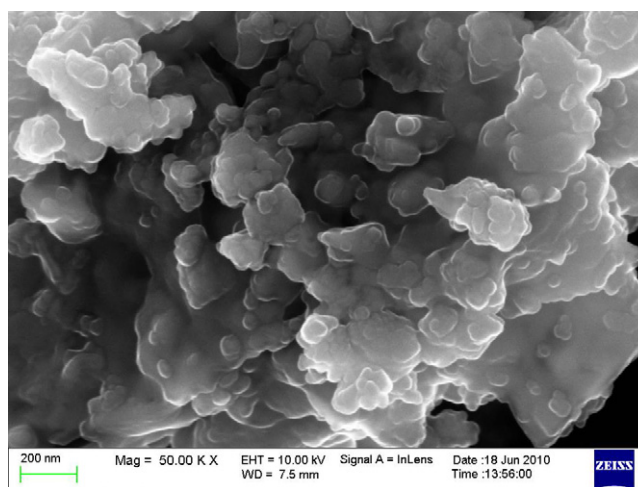**Fig. 5.** FE-SEM micrograph of Fe_3O_4 nanoparticles heated at 700 °C for 2 h.

inset shows magnetization M when magnetic field H was varied from 19,500 Oe to 20,000 Oe to highlight the difference saturation magnetization between the samples. The lower right inset shows a closer look of the zero-field region to highlight the difference coercivity between the samples. The average crystallite size, magnetic properties, lattice parameter and crystalline cell volume of bulk

Fe_3O_4 and Fe_3O_4 nanoparticles processed at different conditions are listed in Table 1. It is clear that all prepared Fe_3O_4 nanoparticles exhibit fine ferromagnetic behavior. The saturation magnetization M_s of Fe_3O_4 nanoparticles increased from 95.12 emu g^{-1} to 97.99 emu g^{-1} with the heating temperature increase from 500 °C to 650 °C. Saturation magnetization M_s of Fe_3O_4 nanoparticles also

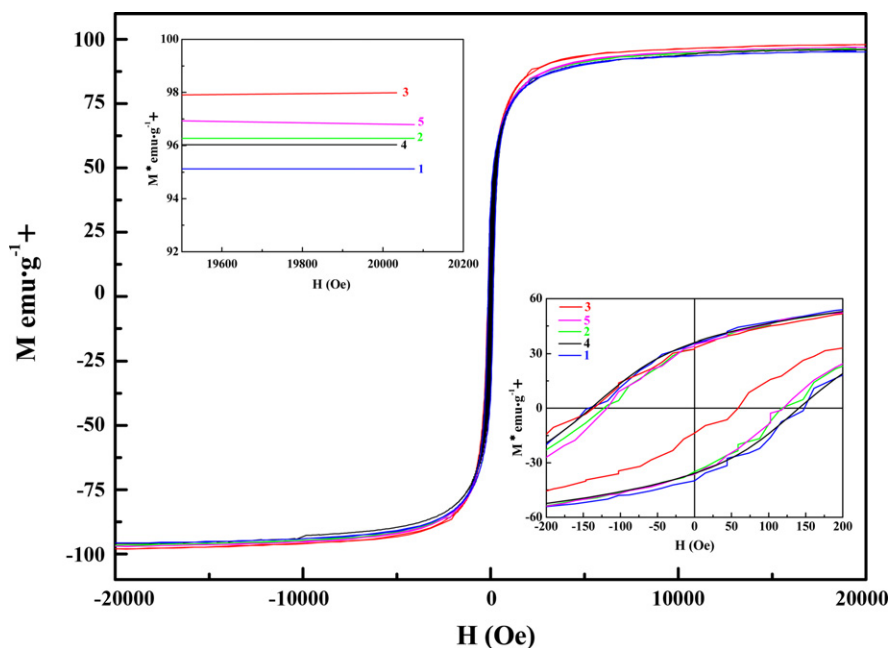**Fig. 6.** Magnetic hysteresis loop of Fe_3O_4 nanoparticles processed at different conditions. The upper left inset shows magnetization M when magnetic field H was varied from 19,500 Oe to 20,000 Oe. The lower right inset shows a closer look of the zero-field region. Here, 1 is the sample heated at 500 °C for 2 h, 2 is the sample heated at 550 °C for 2 h, 3 is the sample heated at 650 °C for 2 h, 4 is the sample heated at 700 °C for 2 h, and 5 is the sample heated at 650 °C for 0.5 h.

Table 1
The average crystallite size, magnetic properties, lattice parameter and volume of crystalline cell of bulk Fe_3O_4 and Fe_3O_4 nanoparticles processed at different conditions.

No.	Samples	M_s (emu g^{-1})	M_r (emu g^{-1})	H_c (Oe)	Average crystallite size (nm)	Lattice parameter (Å)	Volume of crystalline cell (Å^3)
	Bulk Fe_3O_4 [21–25]	92–100	–	–	–	8.396	591.86
1	500 °C for 2 h	95.12 ± 0.01	37.79 ± 0.01	146 ± 1	38 ± 1	8.398 ± 0.001	592.25 ± 0.01
2	550 °C for 2 h	96.27 ± 0.01	34.99 ± 0.01	120 ± 1	42 ± 1	8.404 ± 0.001	593.50 ± 0.01
3	650 °C for 2 h	97.99 ± 0.01	23.44 ± 0.01	98 ± 1	48 ± 1	8.431 ± 0.001	599.34 ± 0.01
4	700 °C for 2 h	96.03 ± 0.01	35.93 ± 0.01	140 ± 1	59 ± 1	8.403 ± 0.001	593.39 ± 0.01
5	650 °C for 0.5 h	96.79 ± 0.01	35.65 ± 0.01	119 ± 1	44 ± 1	8.399 ± 0.001	592.49 ± 0.01

increased from 96.79 emu g^{-1} to 97.99 emu g^{-1} with the holding time increase from 0.5 h to 2 h due to the increase in crystallite size. It is known that saturation magnetization gradually increases with the crystallite size and coercivity which is defined by decreased domain walls displacement as the crystallite size increases in the multi-domain range [21].

However, M_s of sample heated at 700 °C for 2 h is lower than that heated at 650 °C due to excessive grain growth and more aggregation and even partial sintering occur at higher temperature (Fig. 5). The sample heated at 650 °C for 2 h has the largest saturation magnetization (M_s = 97.99 emu g^{-1}), the lowest remaining magnetization (M_r = 23.44 emu g^{-1}) and the lowest coercivity (H_c = 98 Oe). Moreover, the saturation magnetization value of sample 3 (heated at 650 °C for 2 h) is larger than that prepared by other techniques [9–13,26–31] attributed to better microstructure (Fig. 5), crystallinity (Fig. 3) and expanded crystalline cell (Table 1).

Magnetic properties of Fe$_3$O$_4$ powder strongly depend on its crystallinity and synthesis method [32,33]. Fe$_3$O$_4$ crystallizes at ambient conditions in cubic structure (inverse spinel) with $Fd\bar{3}m$ space group in conventional unit cell with iron in two valence states. Tetrahedral A sites are occupied by Fe^{3+}, whereas twice as abundant octahedral B sites are randomly occupied by Fe^{2+} and Fe^{3+}. Magnetic moments on the B sites are antiferromagnetic, while on the A sites they are ferromagnetically aligned. Fe$_3$O$_4$ is ferrimagnetic since the moments at the A and B sites point in opposite directions, giving a net magnetic moment corresponding to that of Fe^{2+} [34]. Differences in crystallization processes could influence Fe^{2+} and Fe^{3+} octahedral sites distribution allowing superexchange interactions between ferric ions [33]. Well-crystallized Fe$_3$O$_4$ particles result in less crystal defects. In addition, the superexchange interaction of Fe–O–Fe was strengthened since expanded crystalline cell and magnetic properties of Fe$_3$O$_4$ nanoparticles were improved. However, crystallinity and microstructure effects on magnetic properties of Fe$_3$O$_4$ powder prepared by carbothermal reduction method are not clear yet.

4. Conclusions

Fe$_3$O$_4$ nanoparticles were prepared by carbothermal reduction method using glucose as carbon source. The effects of heating temperatures and holding time on crystalline phase composition and magnetic properties of Fe$_3$O$_4$ nanoparticles were investigated. Pure Fe$_3$O$_4$ nanoparticles with an average crystallite size of about 48 nm were obtained at heating temperatures higher than 500 °C held for 2 h. However, below 500 °C, only Fe$_3$O$_4$ and Fe$_2$O$_3$ mixed powders were obtained. Moreover, pure Fe$_3$O$_4$ can be synthesized at higher heating temperature (650 °C) for shorter holding time (even 0.5 h), or at lower heating temperature (450 °C) for longer holding time (longer than 6 h) attributed to adequate decomposed carbon source. Furthermore, Fe$_3$O$_4$ heated at 650 °C for 2 h had the highest saturation magnetization (M_s = 97.99 emu g^{-1}) even compared with Fe$_3$O$_4$ prepared by other techniques due to better crystallinity and expanded crystalline cell. This study is helpful for controlled synthesis of pure Fe$_3$O$_4$ by means of the carbothermal reduction method. Produced Fe$_3$O$_4$ nanoparticles can have potential applications in catalysis and biological fields.

References

[1] H. Zeng, J. Li, J.P. Liu, Z.L. Wang, S.H. Sun, Nature 420 (2002) 395.
[2] C.T. Black, C.B. Murray, R.L. Sandstrom, S. Sun, Science 290 (2000) 1131.
[3] T. Atarashi, T. Imai, J. Shimoiizaka, J. Magn. Magn. Mater. 85 (1990) 3.
[4] K. Raj, B. Moskowitz, R. Casciari, J. Magn. Magn. Mater. 149 (1995) 174.
[5] L.X. Tifenauer, A. Tschirky, G. Kuhne, R.Y. Andres, Magn. Reson. Imaging 14 (1996) 391.
[6] D.M. Huang, D.B. Cao, Y.W. Li, H.J. Jiao, J. Phys. Chem. B 110 (2006) 13920–13925.
[7] Z. Berkova, J. Kriz, P. Girman, K. Zacharovova, T. Koblas, E. Dovolilova, F. Saudek, Transplant. Proc. 37 (2005) 3496–3498.
[8] F. Mishima, S. Takeda, Y. Izumi, S. Nishijima, IEEE Trans. Appl. Supercond. 16 (2006) 1539.
[9] W.Q. Jiang, H.C. Yang, S.Y. Yang, H.E. Horng, J.C. Hung, Y.C. Chen, C.Y. Hong, J. Magn. Magn. Mater. 283 (2004) 210–214.
[10] L.Q. Yu, L.J. Zheng, J.X. Yang, Mater. Chem. Phys. 66 (2000) 6–9.
[11] D.E. Zhang, Z.W. Tong, S.Z. Li, X.B. Zhang, A.L. Ying, Mater. Lett. 62 (2008) 4053–4055.
[12] M.Z. Wu, Y. Xing, Y.S. Jia, H.L. Niu, N.P. Qi, J. Ye, Q.W. Chen, Chem. Phys. Lett. 401 (2005) 374.
[13] J. Xu, H.B. Yang, W.Y. Fu, K. Du, Y.M. Sui, J.J. Chen, Y. Zeng, M.H. Li, G.G. Zou, J. Magn. Magn. Mater. 309 (2007) 307–311.
[14] R. Vijayakumar, Y. Koltypin, I. Felner, A. Gedanken, Mater. Sci. Eng. A 286 (2000) 101.
[15] L.Y. Chen, C.L. Zhao, Y. Zhou, H. Peng, Y.Y. Zheng, J. Alloys Compd. 504 (2010) L46–L50.
[16] P. Wang, C. Lee, T. Young, J. Polym. Sci. Part A: Polym. Chem. 43 (2005) 1342.
[17] A.G. Roca, M.P. Morales, K. O'Grady, C.J. Serna, Nanotechnology 17 (2006) 2783.
[18] T. Hyeon, S.S. Lee, J. Park, Y. Chung, H.B. Na, J. Am. Chem. Soc. 123 (2001) 12798.
[19] S.H. Sun, H. Zeng, J. Am. Chem. Soc. 124 (2002) 8204.
[20] H. Wang, P. Hu, D.A. Pan, J.J. Tian, S.G. Zhang, A.A. Volinsky, J. Alloys Compd. 502 (2010) 338–340.
[21] P. Hu, H.B. Yang, D.A. Pan, H. Wang, J.J. Tian, S.G. Zhang, X.F. Wang, A.A. Volinsky, J. Magn. Magn. Mater. 322 (2010) 173–177.
[22] R.M. Cornell, U. Schwertmann, The Iron Oxides: Structure, Properties, Reactions, Occurrences and Uses, Wiley–VCH, Weinheim, Germany, 2003.
[23] R.C. O'Handley, Modern Magnetic Materials: Principles and Applications, Wiley, New York, 2000.
[24] CRC Handbook of Chemistry and Physics, Taylor & Francis CRC Press, Boca Raton, FL, 2004.
[25] Z. Kakol, J.M. Honig, Phys. Rev. B: Condens. Matter Mater. Phys. 40 (1989) 9090.
[26] W.S. Lu, Y.H. Shen, A.J. Xie, W.Q. Zhang, J. Magn. Magn. Mater. 322 (2010) 1828–1833.
[27] X.N. Xu, Y. Wolfus, A. Shaulov, Y. Yeshurun, I. Felner, I. Nowik, Y. Koltypin, A. Gedanken, J. Appl. Phys. 91 (2002) 4611–4616.
[28] W.B. Mi, J.J. Shen, E.Y. Jiang, H.L. Bai, Acta Mater. 55 (2007) 1919–1926.
[29] S.H. Xuan, M.W. Chen, L.Y. Hao, W.Q. Jiang, X.L. Gong, Y. Hu, Z.Y. Chen, J. Magn. Magn. Mater. 320 (2008) 164–170.
[30] L. Cabrera, S. Gutiérrez, P. Herrasti, D. Reyman, Phys. Procs. 3 (2010) 89–94.
[31] J.H. Zhang, J. Du, Y.T. Qian, Q.H. Yin, D.J. Zhang, Mater. Sci. Eng. B 170 (2010) 51–57.
[32] A.S. Teja, P.-Y. Koh, Prog. Cryst. Charact. Mater. 55 (2009) 22–45.
[33] J. Wang, K. Zhang, Z.M. Peng, Q.W. Chen, J. Cryst. Growth 266 (2004) 500–504.
[34] S. Klotz, G. Steinle-Neumann, Th. Strässle, J. Philippe, Th. Hansen, M.J. Wenzel, Phys. Rev. B 77 (2008) 012411.